

Unexpectedly large charge radii of neutron-rich calcium isotopes

R.F. Garcia Ruiz¹, M. L. Bissell^{1,2}, K. Blaum³, A. Ekström^{4,5}, N. Frömmgen⁶, G. Hagen⁴, M. Hammen⁶, K. Hebeler^{7,8}, J.D. Holt¹¹, G.R. Jansen^{4,5}, M. Kowalska⁹, K. Kreim³, W. Nazarewicz^{4,10,12}, R. Neugart^{3,6}, G. Neyens¹, W. Nörtershäuser^{6,7}, T. Papenbrock^{4,5}, J. Papuga¹, A. Schwenk^{7,8}, J. Simonis^{7,8}, K.A. Wendt^{4,5} and D.T. Yordanov^{3,13}

¹KU Leuven, Instituut voor Kern-en Stralingsfysica, B-3001 Leuven, Belgium ²School of Physics and Astronomy, The University of Manchester, Manchester M13 9PL, United Kingdom ³Max-Planck-Institut für Kernphysik, D-69117 Heidelberg, Germany ⁴Physics Division, Oak Ridge National Laboratory, Oak Ridge, Tennessee 37831, USA ⁵Department of Physics and Astronomy, University of Tennessee, Knoxville, Tennessee 37996, USA ⁶Institut für Kernchemie, Universität Mainz, D-55128 Mainz, Germany ⁷Institut für Kernphysik, Technische Universität Darmstadt, 64289 Darmstadt, Germany ⁸ExtreMe Matter Institute EMMI, GSI Helmholtzzentrum für Schwerionenforschung GmbH, 64291 Darmstadt, Germany ⁹CERN, European Organization for Nuclear Research, Physics Department, CH-1211 Geneva 23, Switzerland ¹⁰Department of Physics and Astronomy and NSCL/FRIB Laboratory, Michigan State University, East Lansing, Michigan 48824, USA ¹¹TRIUMF, 4004 Wesbrook Mall, Vancouver, British Columbia, V6T 2A3, Canada ¹²Institute of Theoretical Physics, Faculty of Physics, University of Warsaw, Pasteura 5, PL-02-093 Warsaw, Poland ¹³Institut de Physique Nucléaire d'Orsay, CNRS/IN2P3, Université Paris-Sud, F-91406 Orsay Cedex, France.

Despite being a complex many-body system, the atomic nucleus exhibits simple structures for certain “magic” numbers of protons and neutrons. The calcium chain in particular is both unique and puzzling: evidence of doubly-magic features are known in $^{40,48}\text{Ca}$, and recently suggested in two radioactive isotopes, $^{52,54}\text{Ca}$. Although many properties of experimentally known Ca isotopes have been successfully described by nuclear theory, it is still a challenge to predict their charge radii evolution. Here we present the first measurements of the charge radii of $^{49,51,52}\text{Ca}$, obtained from laser spectroscopy experiments at ISOLDE, CERN. The experimental results are complemented by state-of-the-art theoretical calculations. The large and unexpected increase of the size of the neutron-rich calcium isotopes beyond $N = 28$ challenges the doubly-magic nature of ^{52}Ca and opens new intriguing questions on the evolution of nuclear sizes away from stability, which are of importance for our understanding of neutron-rich atomic nuclei.

Similar to the electrons in the atom, protons and neutrons (nucleons) in atomic nuclei occupy quantum levels that appear in “shells” separated by energy gaps. The number of nucleons that completely fill each shell define the so called “magic” numbers, known in stable nuclei as 2, 8, 20, 28, 50, 82, 126¹. A fundamental understanding of how these magic configurations evolve in unstable neutron-rich nuclei, and how they impact the charge radius, is one of the main challenges of modern experimental and theoretical nuclear physics^{2–9}.

The calcium isotopic chain ($Z = 20$) is a unique nuclear system to study how protons and neutrons interact inside the atomic nucleus: two of its stable isotopes are magic in both their proton and neutron number (^{40}Ca and ^{48}Ca), while experimental evidence of doubly-magic features

in two short-lived calcium isotopes have been reported recently, based on precision measurements of nuclear masses for ^{52}Ca ($N = 32$)⁶ and 2^+ excitation energies for ^{54}Ca ($N = 34$)⁷. Possibly, additional doubly-magic isotopes might exist even further away from stability¹⁰. As a local change in the behaviour of the charge radius is expected in doubly-magic nuclei¹¹, it is important to pin down the charge radius in these exotic isotopes to understand how shell structure evolves and impacts the limits of stability.

Although the average distance between the electrons and the nucleus in an atom is about 5000 times larger than the nuclear radius, the size of the nuclear charge distribution is manifested as a perturbation of the atomic energy levels. A change in the nuclear size between two isotopes gives rise to a shift of the atomic hyperfine structure levels. This shift between two isotopes, commonly known as the isotope shift, $\delta\nu^{A,A'}$, includes a part that is proportional to the change in the nuclear mean square charge radii, $\delta\langle r^2 \rangle^{A,A'}$ (see expression (1) in methods). Isotope shifts of stable Ca isotopes have been extensively studied in the literature¹³, revealing the unusual evolution of their charge radii. Despite an excess of eight neutrons, ^{48}Ca exhibits the striking feature that it has essentially the same charge radius as ^{40}Ca . A fundamental explanation of these anomalous features has been a long-standing problem for nuclear theory for more than three decades (see, e.g.,^{14,15}). Quantitative scenarios have been proposed to account for some of these properties^{14,16,17}, but so far a microscopic description was lacking.

A first estimate for the charge radius of the radioactive ^{49}Ca isotope was based on a failure to observe its resonance in a dedicated measurement of its isotope shift. The resulting conclusion that $\delta\nu^{48,49} \leq 50$ MHz suggested an enormous increase of the charge radius $\delta\langle r^2 \rangle^{48,49} \geq 0.5$ fm²¹⁸, reflecting the strong magicity of ^{48}Ca . So far, the only charge radius measured beyond

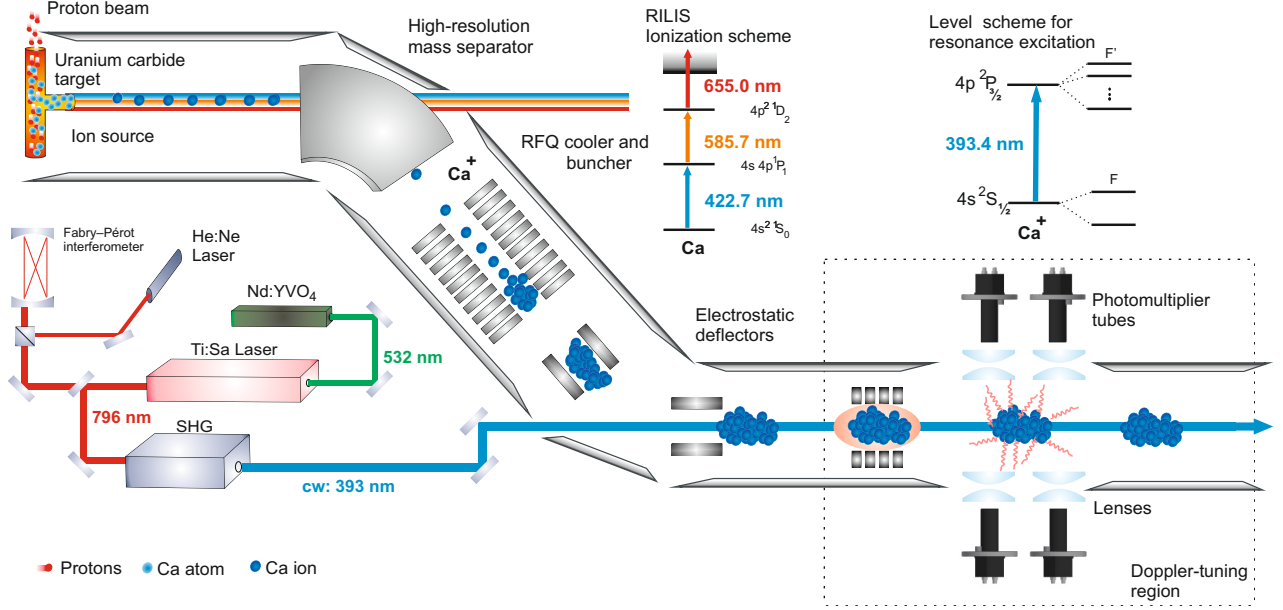


FIG. 1. High-resolution bunched collinear laser spectroscopy at ISOLDE, CERN. Short-lived calcium isotopes are produced from nuclear reactions of high-energy protons impacting on an uranium carbide target. Ca atoms were selectively ionized by using a three-step laser scheme¹². Ions were extracted from the source and mass separated to be injected into a radiofrequency trap, where they are accumulated for typically 100 ms. Bunches of ions were extracted and redirected into the COLLAPS beam line to perform collinear laser spectroscopy experiments. At COLLAPS, the ions are superimposed with a continuous wavelength laser beam to scan the hyperfine structure in the $4s\ ^2S_{1/2} \rightarrow 4p\ ^2P_{3/2}$ transition of Ca^+ (see text for more details).

^{48}Ca has been for ^{50}Ca , resulting in a large increase of $\delta\langle r^2 \rangle^{48,50} = 0.293(37)\text{ fm}^{219}$. These results raised even more exciting questions on the charge radii evolution of Ca isotopes. It suggested that the prominent odd-even staggering of their charge radii could be even more pronounced beyond ^{48}Ca since a reduction of the charge radius for ^{52}Ca would be expected as a consequence of a

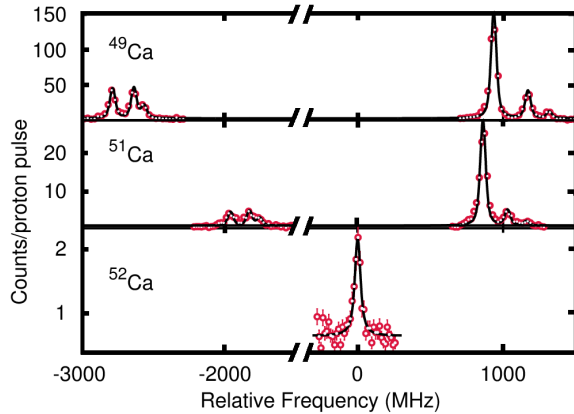


FIG. 2. Examples of hyperfine structure spectra measured for the Ca isotopes in the 393-nm $4s\ ^2S_{1/2} \rightarrow 4p\ ^2P_{3/2}$ ionic transition. The solid lines show the fit with a Voigt profile. Frequency values are relative to the centroid of ^{52}Ca .

suggested doubly-magic nature of this isotope. Thus, the experimental determination of the charge radii of $^{49,51,52}\text{Ca}$ not only addresses fundamental questions regarding the size of atomic nuclei, but are also important for understanding the possible doubly-magic character of ^{52}Ca . By using high-resolution bunched-beam collinear laser spectroscopy at ISOLDE, CERN, changes in the charge radii for $^{40-52}\text{Ca}$ isotopes were obtained from the measured optical isotope shifts (see Table I). With a production yield of only a few hundred ions per second, our measurement of ^{52}Ca represents one of the highest sensitivities ever reached by using fluorescence detection techniques.

The isotope shift is typically 10^6 times smaller than the absolute transition frequency between two atomic levels, and the relevant part is in turn only a small fraction of the total shift. Thus a measurement of such a tiny change is only possible by using ultra-high resolution techniques. Collinear laser spectroscopy has been established as a unique method to reach such high resolution and has been applied with different detection schemes to study a variety of isotopes²²⁻²⁴.

A major challenge of exotic nuclei is that they are produced in very low quantities and exist only for a fraction of a second. Therefore, continuous improvements have been made during the past decades to enhance the exper-

TABLE I. **Measured isotope shifts and corresponding rms charge radii.** Statistical and systematic uncertainties are given in round and squared brackets, respectively.

A	$\delta\nu^{40,A}$ (MHz)			$\delta\langle r^2 \rangle$ (fm ²)		
	This work	Literature		This work	Literature	
40	0	0 ^a	0 ^b	0 ^c	0 ^d	0 ^e
42	—	426.4(15)[10]	425(4)[4]		0.203(15)	0.215(5)
43	683.0(12)[16]		672(9)[6]	0.114(4)[8]	0.125(30)	0.125(3)
44	851.1(6)[21]	850.1(10)[20]	842(3)[8]	0.288(2)[6]	0.280(11)	0.283(6)
45	1103.5(7)[25]		1091(4)[10]	0.125(3)[8]	0.126(15)	0.119(6)
46	1301.0(6)[30]		1287(3)[12]	0.125(2)[8]	0.124(11)	0.124(5)
47	1524.8(8)[35]			0.002(3)[9]		0.005(13)
48	1706.5(8)[38]	1710.6(35)[42]	1696(4)[16]	0.001(3)[10]	−0.022(15)	−0.004(6)
49	1854.7(10)[43]			0.098(4)[12]		
50	1969.2(9)[47]		1951(9)[20]	0.291(3)[12]	0.276(34)	
51	2102.6(9)[51]			0.392(3)[13]		
52	2219.2(14)[56]			0.531(5)[15]		

^a High-precision measurements of isotope shifts of stable Ca isotopes²⁰.

^b Data from Ref¹⁹.

^c Values of $K_{SMS} = -8.8(5)$ GHz u and $F = -276(8)$ MHz/fm² were taken from the King-plot results (see methods). In square brackets are listed the systematic errors associated to these factors, which are related to the uncertainty of the kinetic energy of the ion beam.

^d Recalculated from isotope shift values reported in¹⁹ using the newly reported mass values²¹.

^e Taken from Ref.¹³.

imental sensitivity, without sacrificing resolution. Since the introduction of an ion cooler-buncher for collinear spectroscopy that allows bunching radioactive beams²⁵, the sensitivity of the conventional fluorescence laser spectroscopy has been improved by two to three orders of magnitude. It is now possible to routinely perform experiments with beams of $\sim 10^4$ ions/s²⁶. In this work, we have further optimized the photon detection sensitivity and at the same time reduced further the photon background events⁸, now allowing to study calcium isotopes produced with a yield of only a few hundred ions per second. While preserving the high resolution, this sensitivity surpasses the previous limit by two orders of magnitude, achieved by an ultra-sensitive particle detection technique employed on Ca isotopes¹⁹.

The short-lived Ca isotopes studied in this work were produced at the ISOLDE on-line isotope separator, located at the European Center for Nuclear Research, CERN. High-energy proton pulses with intensities of $\sim 3 \times 10^{13}$ protons/pulse at 1.4 GeV impinged every 2.4 seconds on an uranium carbide target to create radioactive species of a wide range of chemical elements. The Ca isotopes were selected from the reaction products by using a three-step laser ionization scheme provided by the Resonance Ionization Laser Ion Source (RILIS)¹². A detailed sketch of the different experimental processes from the ion beam production to the fluorescence detection is shown in Fig. 1.

After selective ionization, Ca ions (Ca⁺) were extracted from the ion source and accelerated up to 40 keV. The isotope of interest was mass-separated by using the High-Resolution Mass Separator (HRS). The selected isotopes were injected into a gas-filled radiofrequency trap

(RFQ) to accumulate the incoming ions. After a few milliseconds, bunches of ions of $\sim 5\mu$ s temporal width were extracted and redirected into a dedicated beam line for collinear laser spectroscopy experiments (COLLAPS). At COLLAPS, the ion beam was superimposed with a continuous wave laser beam fixed at 393-nm wavelength (see methods), close to the $4s\ ^2S_{1/2} \rightarrow 4p\ ^2P_{3/2}$ transition in the Ca⁺. The laser frequency was fixed to a constant value, while the ion velocity was varied inside the optical detection region. A change in the ion velocity corresponds to a variation of laser frequency in the ion rest frame. This Doppler tuning of the laser frequency was used to scan the hyperfine structure (hfs) components of the $4s\ ^2S_{1/2} \rightarrow 4p\ ^2P_{3/2}$ transition. At resonance frequencies, transitions between different hfs levels were excited, and subsequently the fluorescence photons were detected by a light collection system consisting of four lenses and photomultiplier tubes (PMT) (see Refs.⁸ for details). The photon signals were accepted only when the ion bunch passed in front of the light collection region, reducing the background counts from scattered laser light and PMT dark counts by a factor of $\sim 10^4$. A sample of the hfs spectra measured during the experiment is shown in Fig. 2.

The isotope shifts were extracted from the fit of the hfs experimental spectra, assuming multiple Voigt profiles in the χ^2 -minimization (see methods). The measured isotope shift relative to the reference isotope ⁴⁰Ca, and the corresponding change in the mean-square charge radius are shown in Table I. Statistical errors (parentheses) correspond to the uncertainty in the determination of the peak positions in the hfs spectra. The systematic

errors in the isotope shift (square brackets) are mainly due to the uncertainty in the beam energy, which is also the main contribution to the uncertainty in the charge radius. Independent high-precision measurements of isotope shifts on stable Ca isotopes²⁰ were used for an accurate determination of the kinetic energy of each isotope. The stability of the beam energy was controlled by measuring the stable ^{40}Ca , before and after the measurement of each isotope of interest.

Our experimental results (Table I and Fig. 3) show that the root-mean-square (rms) charge radius of ^{49}Ca presents a considerable increase with respect to ^{48}Ca , $\delta\langle r^2 \rangle^{48,49} = 0.097(4) \text{ fm}^2$, but much smaller than previously suggested¹⁸. The increase continues towards $N = 32$, resulting in a very large charge radius for ^{52}Ca , with an increase relative to ^{48}Ca of $\delta\langle r^2 \rangle^{48,52} = 0.530(5) \text{ fm}^2$. This increase observed beyond the neutron number $N = 28$ is as large as the values observed for open-shell nuclei like Fe^{27} , where there is not a sizable shell gap at $N = 32$. Thus, the charge radius of ^{52}Ca is found to be much larger than expected for a doubly-magic nucleus.

With advances in chiral effective field theory (EFT) and the development of powerful many-body methods, nuclear structure theory has entered a new era in recent years. Chiral EFT allows to systematically derive nuclear forces in terms of low-energy degrees of freedom, nucleons and pions, based on the symmetries of the fundamental theory, Quantum Chromodynamics. Chiral EFT provides systematically improvable Hamiltonians, explains naturally the hierarchy of two-, three-, and higher-body forces, and allows to estimate theoretical uncertainties²⁸.

Ab initio calculations based on chiral EFT interactions are able to correctly predict properties of light nuclei³¹ and oxygen isotopes³². In addition, many-body calculations starting from a ^{40}Ca core provide an excellent description of the binding energies of neutron-rich Ca isotopes⁶, 2^+ excitation energies^{4,5,33} and ground-state electromagnetic moments³⁴. However, there are also clear indications for deficiencies of some chiral EFT interactions: ground-state energies of heavier nuclei turn out to be systematically too large and radii are significantly too small^{9,35}.

Very recently, this problem was addressed by an optimization of chiral EFT interactions⁹ that also included binding energies and radii of selected nuclei up to mass number $A = 25$ in addition to data from two- and few-body systems. Ab initio coupled-cluster calculations based on the resulting interaction (NNLO_{sat}) accurately reproduce both charge radii and binding energies of nuclei up to ^{40}Ca , and the empirical saturation point of symmetric nuclear matter. In addition to NNLO_{sat} , we employ two chiral interactions³⁶, SRG1 and SRG2, derived from renormalization group techniques³⁷ (see methods for details), which are fit only to properties of $A \leq 4$ and predict nuclear matter saturation within theoretical uncertainties.

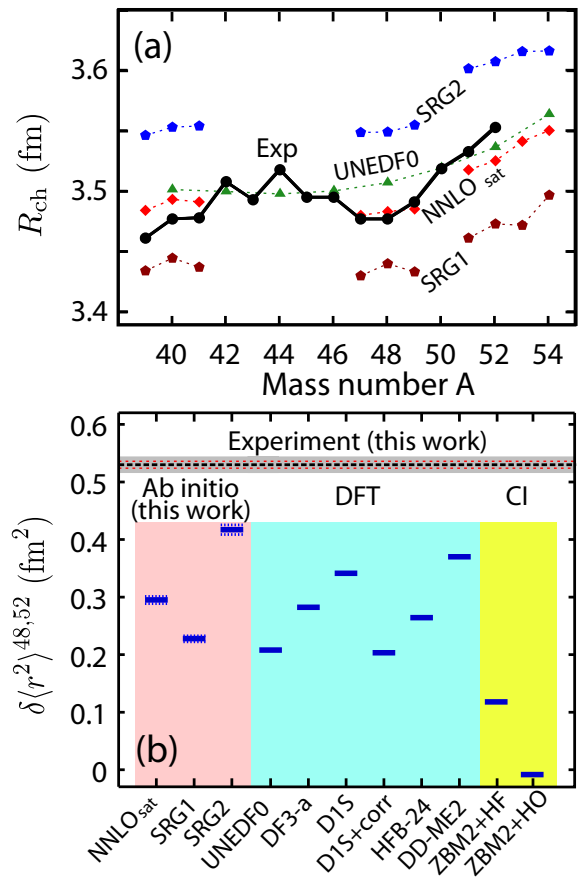


FIG. 3. Charge radii of Ca isotopes. (a) Experimental charge radii compared to ab initio calculations with chiral EFT interactions NNLO_{sat} , SRG1, SRG2, as well as DFT calculations with the UNEDF0 functional. Experimental error bars are smaller than the symbols. The absolute values were obtained from the reference radius of ^{40}Ca ($R_{\text{ch}} = 3.478(2) \text{ fm}$)²⁷. The values of ^{39}Ca and $^{41,42}\text{Ca}$ are taken from Ref.²⁹ and Ref.³⁰, respectively. A systematic theoretical uncertainty of 1% is estimated for the absolute values due to the truncation level of the coupled-cluster method and the finite basis-space employed in the computation. (b) Experimental rms charge radius in ^{52}Ca relative to that in ^{48}Ca compared to the ab initio results as well as those of representative density functional theory (DFT) and configuration interaction (CI) calculations. The systematic uncertainties in the theoretical predictions are largely cancelled when the differences between rms charge radii are calculated (dotted horizontal blue lines). Experimental uncertainties are represented by the horizontal red lines (statistical) and the gray shaded band (systematic).

In Fig. 3 we compare the experimental results to the charge radii obtained in our ab initio calculations and to other theoretical predictions. Figure 3 (a) shows that our calculations correctly yield similar charge radii for ^{40}Ca and $^{47,48}\text{Ca}$ for the chiral EFT interactions employed. These calculations are based on the single-reference coupled-cluster method, which is ideally suited for nuclei with at most one or two nucleons outside a

closed (sub-) shell³⁸. Thus, we do not give theoretical results for the mid-shell isotopes ^{42–46}Ca and ⁵⁰Ca. We note that absolute values of charge radii are very well reproduced by NNLO_{sat}. The interactions SRG1 and SRG2 also reproduce well the overall trend, but as they were not optimized to saturation properties can give either somewhat too low or too high saturation densities, corresponding to larger or smaller charge radii. Also shown are nuclear DFT results obtained with the Skyrme energy density functional UNEDF0³⁹, which fails to describe the fine details of the experimental trend.

Figure 3 (b) shows the difference in rms charge radii between ⁵²Ca and ⁴⁸Ca predicted with different methods and models; all being representative of modern approaches to charge radii. In general, for neutron-rich isotopes beyond ⁴⁸Ca, our ab initio calculations consistently predict an increase in charge radii for ^{50,52}Ca but fail short of describing the data. Similarly, DFT predictions with various models^{40–45}; configuration interaction (CI) calculations⁴⁵ obtained from large-scale shell-model calculations with the ZBM2 interaction^{14,46} using Skyrme-Hartree-Fock (ZBM2+HF) and harmonic oscillator (ZBM2+HO) wave functions, all considerably underestimate the large charge radius of ⁵²Ca. The standard explanation involving quadrupolar correlations^{14,45} does not seem to improve this, as can be seen by comparing the D1S and D1S plus quadrupolar correlations (D1S+corr) results⁴² in Fig. 3 (b). (For more discussion of the impact of dynamical quadrupole and octupole effects on charge radii in the Ca chain, see also Ref.¹⁷.) Thus, our experimental results are truly unexpected. Speculating about the reason for these theoretical shortcomings we note that all theoretical approaches are lacking in the description of deformed intruder states associated with complex configurations.

To assess the impact of core breaking effects, which turned out to be important for the description of electromagnetic moments in this region³⁴, we studied the proton occupancies of natural orbitals above the naively filled $Z = 20$ shell. Our ab initio calculations show a weak, but gradual erosion of the proton core as neutrons are added. While this defies the simple pattern of a rigid proton core expected for the magic Ca isotopes, the estimated magnitude of core breaking effects, including coupling to the neutrons, is not sufficient to explain the large charge radius of ⁵²Ca.

In summary, the charge radii of ^{49,51,52}Ca were measured for the first time, extending the picture for the evolution of charge radii over three neutron shell closures; a unique scenario found in the entire nuclear chart. We find that between ⁴⁸Ca and ⁵²Ca the charge radius exhibits a strong increase that considerably exceeds theoretical predictions. This is a surprising finding, considering that ⁴⁰Ca and ⁴⁸Ca have similar charge radii¹⁹, which are significantly smaller than the charge radius of ⁵²Ca. Our measurements are complemented by ab initio calculations

that reproduce the similarities of charge radii in ^{40,48}Ca but cannot account for the unexpected increase in R_{ch} to ⁵²Ca. These calculations also show an increase in proton occupancies outside the $Z = 20$ core as more neutrons are added to ⁴⁰Ca, hinting at a progressive weakening of the $Z = 20$ shell closure in the neutron-rich calciums. Future experiments aim at extending the current studies to isotopes even further away from stability, especially for the possibly doubly-magic nucleus ⁵⁴Ca⁷. These results open intriguing questions on the evolution of charge radii away from stability and constitute a major challenge in the search of a unified description of the atomic nucleus.

METHODS

Laser setup The continuous wave laser beam at 393-nm wavelength was obtained from a second-harmonic generation of a Ti:Sa laser output, pumped with 532 nm light from a cw Nd:YVO₄ laser. To reduce the laser frequency drift to less than 10 MHz per day, the laser frequency was locked to a Fabry-Perrot interferometer, which was in turn locked to a polarization-stabilized HeNe laser (see Figure 1).

Chiral EFT interactions The *ab initio* calculations in this work are based on interactions derived within chiral effective field theory. The interaction NNLO_{sat} includes contributions to nucleon-nucleon and three-nucleon forces up to third order in the chiral expansion, which have been fitted to selected properties of nuclei up to ²⁴O, so as to include information on saturation properties (see Ref.⁹ for details). The interactions SRG1 and SRG2 are derived from the fourth-order chiral nucleon-nucleon interaction of Ref.⁴⁷ by performing an evolution to lower resolution scales via the the similarity renormalization group³⁶. The three-nucleon interactions include contributions up to third order in the chiral expansion and are fit to the binding energy of ³H and the charge radius of ⁴He at the low resolution scales. The interaction SRG1 refers to an interaction at the the resolution scales $\lambda/\Lambda_{3\text{NF}} = 2.8/2.0 \text{ fm}^{-1}$ (EM c_i 's) and SRG2 to $\lambda/\Lambda_{3\text{NF}} = 2.0/2.0 \text{ fm}^{-1}$ (PWA c_i 's) (see Table 1 in Ref.³⁶).

Coupled-cluster calculations Our coupled-cluster (CC) calculations are performed starting from a closed-shell Hartree-Fock reference state computed from 15 harmonic-oscillator shells with an oscillator frequency of $\hbar\Omega = 22 \text{ MeV}$. In CC theory correlations are included via a similarity transformation, which generates particle-hole excitations to all orders in perturbation theory. In our calculations the cluster operator is truncated at the singles and doubles level (CCSD), and also includes triples excitations in a nonperturbative but approximate way (see Ref.³⁸ for details). Contributions from three-nucleon forces are taken into account up to $E_{3\text{max}} = 18 \hbar\Omega$ for NNLO_{sat} and $E_{3\text{max}} = 16 \hbar\Omega$ for SRG1 and SRG2 in the normal-ordering approximation, which has been demonstrated to be an excellent approximation for medium-mass nuclei⁴⁸. Based on the size-extensivity of the CC method, the uncertainty of the radius results is estimated to 1% in the CCSD approximation. The uncertainties of the *ab-initio* results shown in Fig. 3 (b) are very small, because they are differences of correlated and very small (1%) uncertainties of each individual radius. We find 0.006 fm^2 , 0.005 fm^2 , and 0.008 fm^2 for the uncertainties of $\delta\langle r^2 \rangle$ ^{48,52} for the interactions NNLO_{sat}, SRG1, and SRG2, respectively.

The results for the charge radii are computed from the point-proton radius starting from the intrinsic operator. We then correct the point-proton radius for the finite proton and neutron charge sizes, for the relativistic

Darwin-Foldy term, and the spin-orbit correction. The latter is calculated consistently in CC theory. Finally, we note that the DFT results also include this spin-orbit correction. If not added in the original reference, we adopt spin-orbit corrections given by the mean of CC theory and relativistic mean-field theory.

Data analysis The measured hyperfine structure spectra were fitted with Voigt profiles of common widths for the different hfs components. The hfs centroid obtained for each isotope were used to extract the isotope shifts, $\delta\nu^{A,A'}$, and calculate the corresponding change in rms charge radius, $\delta\langle r^2 \rangle^{A,A'}$, following the expression

$$\delta\langle r^2 \rangle^{A,A'} = \langle r^2 \rangle^{A'} - \langle r^2 \rangle^A = \frac{1}{F} \left(\delta\nu^{A,A'} - K_{\text{MS}} \frac{M_{A'} - M_A}{M_A M_{A'}} \right). \quad (1)$$

The mass shift, K_{MS} , is the sum of the normal mass shift, K_{NMS} , and the specific mass shift, K_{SMS} . The value $K_{\text{NMS}} = 417.97 \text{ GHz u}$ was obtained from the energy of the $4s \ ^2S_{1/2} \rightarrow 4p \ ^2P_{3/2}$ transition of Ca⁺. The electronic field factor, F , and the specific mass shift factor, K_{SMS} , were obtained by comparing with independent measurements of charge radii in a King-plot analysis¹³. The results: $F = -276(8) \text{ MHz/fm}^2$ and $K_{\text{SMS}} = -8.8(5) \text{ GHz u}$, are in good agreement with the literature values³⁰.

Acknowledgments This work was supported by the IAP-project P7/12, the FWO-Vlaanderen, GOA grants 10/010 and 15/010 from KU Leuven, the Max-Planck Society, the ERC Grant No. 307986 STRONGINT, the BMBF contract 05P12RDCIC and 05P15RDCIA, the U.S. Department of Energy, Office of Science, Office of Nuclear Physics under Award Numbers DEFG02-96ER40963 (University of Tennessee), DE-SC0013365 (Michigan State University), DE-SC0008499 and DE-SC0008511 (NUCLEI SciDAC collaboration), the Field Work Proposal ERKBP57 at Oak Ridge National Laboratory (ORNL), and Contract No. DE-AC05-00OR22725 (ORNL). Computer time was provided by the Innovative and Novel Computational Impact on Theory and Experiment (INCITE) program. This research used resources of the Oak Ridge Leadership Computing Facility at ORNL, and used computational resources of the National Center for Computational Sciences, the National Institute for Computational Sciences. We thank Javier Menéndez for very useful discussions. We would like to thank the ISOLDE technical group for their support and assistance.

Author contributions R.F.G.R., M.L.B., N.F., M.H., M.K., K.K., R.N., W.Nö., J.P., and D.T.Y. performed the experiment. R.F.G.R. performed the data analysis and prepared the figures. G.H. and G.R.J. performed the coupled-cluster calculations. R.F.G.R., K.B., G.H., K.H., G.N., W.Na., W.Nö., T.P., and A.S. prepared the manuscript. All authors discussed the results and contributed to the manuscript at all stages.

Author information Reprints and permissions information is available at www.nature.com/reprints.

The authors declare no competing financial interests. Readers are welcome to comment on the on-

line version of the paper. Correspondence and requests for materials should be addressed to R.F.G.R (ronald.fernando.garcia.ruiz@cern.ch)

- ¹ Goeppert Mayer, M. On closed shells in nuclei. *Phys. Rev. C* **75**, 1969 (1949).
- ² Fridmann, J. *et al.* Magic nucleus ^{42}S . *Nature* **435**, 922 (2005).
- ³ Jones, K. *et al.* The magic nature of ^{133}Sn explored through the single-particle states of ^{133}Sn . *Nature* **465**, 454 (2010).
- ⁴ Holt, J. D., Otsuka, T., Schwenk, A. & Suzuki, T. Three-body forces and shell structure in calcium isotopes. *J. Phys. G* **39**, 085111 (2012).
- ⁵ Hagen, G., Hjorth-Jensen, M., Jansen, G. R., Machleidt, R. & Papenbrock, T. Evolution of shell structure in neutron-rich calcium isotopes. *Phys. Rev. Lett.* **109**, 032502 (2012).
- ⁶ Wienholtz, F. *et al.* Masses of exotic calcium isotopes pin down nuclear forces. *Nature* **498**, 346 (2013).
- ⁷ Steppenbeck, D. *et al.* Evidence for a new nuclear 'magic number' from the level structure of ^{54}Ca . *Nature* **502**, 207 (2013).
- ⁸ Kreim, K. *et al.* Nuclear charge radii of potassium isotopes beyond $N=28$. *Phys. Lett. B* **731**, 97 (2014).
- ⁹ Ekström, A. *et al.* Accurate nuclear radii and binding energies from a chiral interaction. *Phys. Rev. C* **91**, 051301 (2015).
- ¹⁰ Gade, A. *et al.* Nuclear structure towards $N = 40$ ^{60}Ca : In-beam γ -ray spectroscopy of $^{58,60}\text{Ti}$. *Phys. Rev. Lett.* **112**, 112503 (2014).
- ¹¹ Angeli, I. *et al.* N and Z dependence of nuclear charge radii. *J. Phys. G* **36**, 085102 (2009).
- ¹² Marsh, B. *et al.* RILIS applications at CERN/ISOLDE. *Hyper. Int.* **227**, 101 (2014).
- ¹³ Palmer, C. W. P. *et al.* Laser spectroscopy of calcium isotopes. *J. Phys. B* **17**, 2197 (1984).
- ¹⁴ Caurier, E., Langanke, K., Martínez-Pinedo, G., Nowacki, F. & Vogel, P. Shell model description of isotope shifts in calcium. *Phys. Lett. B* **522**, 240 (2001).
- ¹⁵ Bender, M., Heenen, P.-H. & Reinhard, P.-G. Self-consistent mean-field models for nuclear structure. *Rev. Mod. Phys.* **75**, 121 (2003).
- ¹⁶ Talmi, I. On the odd-even effect in the charge radii of isotopes. *Nucl. Phys. A* **423**, 189 (1984).
- ¹⁷ Fayans, S., Tolokonnikov, S., Trykov, E. & Zawischa, D. Nuclear isotope shifts within the local energy-density functional approach. *Nucl. Phys. A* **676**, 49 (2000).
- ¹⁸ Andl, A. *et al.* Isotope shifts and hyperfine structure of the $4s^2\ ^1S_0$ - $4s4p\ ^1P_1$ transition in calcium isotopes. *Phys. Rev. C* **26**, 2194 (1982).
- ¹⁹ Vermeeren, L. *et al.* Ultrasensitive radioactive detection of collinear-laser optical pumping: Measurement of the nuclear charge radius of ^{50}Ca . *Phys. Rev. Lett.* **68**, 1679 (1992).
- ²⁰ Gorges, C. *et al.* High-precision isotope shift measurements of stable Ca isotopes. *Submitted* (2015).
- ²¹ Wang, M. *et al.* The AME2012 atomic mass evaluation. *Chinese Phys. C* **36**, 1603 (2012).
- ²² Geithner, W. *et al.* Measurement of nuclear moments and radii by collinear laser spectroscopy and by β -NMR spectroscopy. *Hyper. Int.* **129**, 271 (2000).
- ²³ Cheal, B. & Flanagan, K. Progress in laser spectroscopy at radioactive ion beam facilities. *J. Phys. G: Nucl. Part. Phys.* **37**, 113101 (2010).
- ²⁴ Blaum, K., Dilling, J. & Nörtershäuser, W. Precision atomic physics techniques for nuclear physics with radioactive beams. *Phys. Scr.* **T152**, 014017 (2013).
- ²⁵ Nieminen, A. *et al.* On-line ion cooling and bunching for collinear laser spectroscopy. *Phys. Rev. Lett.* **88**, 094801 (2002).
- ²⁶ Vingerhoets, P. *et al.* Nuclear spins, magnetic moments, and quadrupole moments of Cu isotopes from $N=28$ to $N=46$: Probes for core polarization effects. *Phys. Rev. C* **82**, 064311 (2010).
- ²⁷ Fricke, G. & Heilig, K. *Nuclear Charge Radii* (Springer, 2004).
- ²⁸ Epelbaum, E., Hammer, H.-W. & Meißner, U.-G. Modern theory of nuclear force. *Rev. Mod. Phys.* **81**, 1773 (2009).
- ²⁹ Vermeeren, L. *et al.* The mean square nuclear charge radius of ^{39}Ca . *J. Phys. G: Nucl. Part. Phys.* **22**, 1517 (1996).
- ³⁰ Martensson-Pendrill, A. M. *et al.* Isotope shifts and nuclear-charge radii in singly ionized $^{40-48}\text{Ca}$. *Phys. Rev. A* **45**, 4675 (1992).
- ³¹ Navrátil, P., Gueorguiev, V. G., Vary, J. P., Ormand, W. E. & Nogga, A. Structure of $A = 10 - 13$ nuclei with two- plus three-nucleon interactions from chiral effective field theory. *Phys. Rev. Lett.* **99**, 042501 (2007).
- ³² Hergert, H., Binder, S., Calci, A., Langhammer, J. & Roth, R. Ab Initio Calculations of Even Oxygen Isotopes with Chiral Two-Plus-Three-Nucleon Interactions. *Phys. Rev. Lett.* **110**, 242501 (2013).
- ³³ Coraggio, L., Covello, A., Gargano, A. & Itaco, N. Spectroscopic study of neutron-rich calcium isotopes with a realistic shell-model interaction. *Phys. Rev. C* **80**, 044311 (2009).
- ³⁴ Garcia Ruiz, R. F. *et al.* Ground-state electromagnetic moments of calcium isotopes. *Phys. Rev. C* **91**, 041304(R) (2015).
- ³⁵ Binder, S., Langhammer, J., Calci, A. & Roth, R. Ab initio path to heavy nuclei. *Phys. Lett. B* **736**, 119 (2014).
- ³⁶ Hebeler, K., Bogner, S., Furnstahl, R., Nogga, A. & Schwenk, A. Improved nuclear matter calculations from chiral low-momentum interactions. *Phys. Rev. C* **83**, 031301(R) (2011).
- ³⁷ Furnstahl, R. & Hebeler, K. New applications of renormalization group methods in nuclear physics. *Rep. Prog. Phys.* **76**, 126301 (2013).
- ³⁸ Hagen, G., Papenbrock, T., Hjorth-Jensen, M. & Dean, D. Coupled-cluster computations of atomic nuclei. *Rep. Prog. Phys.* **77**, 096302 (2014).
- ³⁹ Kortelainen, M. *et al.* Nuclear energy density optimization.

- Phys. Rev. C* **82**, 024313 (2010).
- ⁴⁰ Erler, J. *et al.* The limits of the nuclear landscape. *Nature* **486**, 509 (2012).
- ⁴¹ Saperstein, E. & Tolokonnikov, S. Self-consistent theory of finite fermi systems and radii of nuclei. *Phys. Atom. Nucl.* **74**, 1277 (2011).
- ⁴² Delaroche, J.-P. *et al.* Structure of even-even nuclei using a mapped collective hamiltonian and the D1S Gogny interaction. *Phys. Rev. C* **81**, 014303 (2010).
- ⁴³ Roca-Maza, X., Viñas, X., Centelles, M., Ring, P. & Schuck, P. Relativistic mean-field interaction with density-dependent meson-nucleon vertices based on microscopical calculations. *Phys. Rev. C* **84**, 054309 (2011).
- ⁴⁴ Goriely, S., Chamel, N. & Pearson, J. M. Further explorations of Skyrme-Hartree-Fock-Bogoliubov mass formulas. XIII. the 2012 atomic mass evaluation and the symmetry coefficient. *Phys. Rev. C* **88**, 024308 (2013).
- ⁴⁵ Rossi, D. M. *et al.* Charge radii of neutron-deficient ^{36}K and ^{37}K . *Phys. Rev. C* **92**, 014305 (2015).
- ⁴⁶ Bissell, M. L. *et al.* Proton-neutron pairing correlations in the self-conjugate nucleus ^{38}K probed via a direct measurement of the isomer shift. *Phys. Rev. Lett.* **113**, 052502 (2014).
- ⁴⁷ Entem, D. & Machleidt, R. Accurate charge-dependent nucleon-nucleon potential at fourth order of chiral perturbation theory. *Phys. Rev. C* **68**, 041001(R) (2003).
- ⁴⁸ Roth, R. *et al.* Medium-mass nuclei with normal-ordered chiral NN+3N interactions. *Phys. Rev. Lett.* **109**, 052501 (2012).